-RESEARCH PAPER-

International Journal of Mining and Geo-Engineering

IJMGE

IJMGE 57-4 (2023) 397-404

DOI: 10.22059/IJMGE.2023.355656.595039

Mineral potential mapping of porphyry copper deposit by translating the mineral system using soil geochemistry data at Kahang, Iran

Saeid Hajsadeghi [a], Mirsaleh Mirmohammadi [a, *], Omid Asghari [b]

[a] *School of Mining Engineering, College of Engineering, University of Tehran, Tehran.*

[b] *Simulation and Data Processing Laboratory, School of Mining Engineering, University of Tehran, Tehran, Iran.*

Article History:

Received: 19 February2023.

Revised: 09 July 2023.

Accepted: 15 July 2023.

ABSTRACT

Identification of geochemical anomalies is a critical task in mineral exploration targeting. Decades of research and technology have resulted in new algorithms and techniques for recognizing anomaly detection methods at various scales and sample media. However, algorithms cannot always reveal the true nature of geological processes. The mineral system concept may contribute to a better understanding of the geological processes required to form and preserve ore deposits at all spatial and temporal scales. The mineral systems concept investigates the geochemical processes occurring within mineral subsystems in soil samples from the porphyry prospect area. The Cu/(Al + Ca) index was used to compare Cu, Mo, and (Pb* Zn)/(Cu*Mo) to highlight the region of interest for mineral potential mapping and pioneer borehole drilling based on fluid-rock interaction and secondary processes (e.g., alteration, weathering, and leaching). Exploratory boreholes validate a better performing Cu/(Al + Ca) index for detecting and refining soil geochemical anomalies.

Keywords: *soil geochemistry, porphyry copper deposit, mineral system concept, Kahang porphyry copper deposit.*

1. Introduction

Due to the increasing use of mineral exploration methods over the last few decades, the mineral systems concept [1-2] has generated increased awareness and understanding of the range of geological processes required to form and preserve ore deposits at all scales, both spatially and temporally [3-7].

Five critical processes can be considered in the context of the mineral system [1-2]:

- 1- Source: Geological processes are required to extract ore-forming fluids from their source.
- 2- Transport: Geological processes necessary for the ore-forming fluids to travel from the source to the trap.
- 3- Trap: Geological processes necessary for concentrating ore-forming fluids into physically or chemically responsive localities capable of storing significant quantities of ore and gangue.
- 4- Deposition: Refers to the geological processes required for extracting metals effectively from fluids that flow through traps.
- 5- Preservation: Involves the geological processes necessary for maintaining and safeguarding accumulated metals.

Yousefi et al [8] introduced the concept of exploration information systems (EIS) as a novel information system that combines the conceptual mineral deposit model with existing data to aid in exploration targeting using the mineral system. Within an EIS, mineral systems are categorized as scale-dependent subsystems that play a role in the creation of mineral deposits. These subsystems encompass various components, such as:

- (i) Pre-mineralization subsystems: Those associated with mantle or crustal fertility or ground preparation that may have functioned or existed for an extended period before mineralization.
- (ii) Syn-mineralization subsystems: These subsystems were connected to the ore-forming processes that controlled mineralization.
- (iii) Post-mineralization subsystems: Those involved in exhumation, preservation, upgrading, or secondary dispersion.

Although pre- and syn-mineralization subsystems are usually taken into account when studying mineral systems, it is important not to disregard the impact of post-mineralization subsystems. In addition to understanding mineral systems, another challenge lies in converting mineral subsystems into criteria that can be mapped (such as proxies, exploration criteria, and mappable features) [7]. This problem could be resolved if each subsystem leaves identifiable "footprints" in geological, geophysical, and geochemical datasets at both regional and craton scales [9].

Geochemical data are an important and efficient exploration tool that can be scaled up to gain a comprehensive understanding of the processes involved in ore formation within a mineralized district [10-13]. Geochemical datasets are critical for defining lithological units and interpreting stratigraphy more precisely by better distinguishing rock fertility, ore-forming fluid pathways, fluid-rock interaction, and possible trap sites, Moreover, identifying the dispersion patterns of certain elements or geochemical anomalies can help identify potential exploration targets. [10-11, 14-15]. A geochemical anomaly can be defined as:

* Corresponding author. *E-mail address:* m.mirmohammadi@ut.ac.ir (M. Mirmohammadi).

(i) A significant difference in the concentration of geochemical pathfinder elements associated with specific deposits from the background value.

Recent studies have typically focused on developing novel algorithms or techniques for detecting anomalies across a range of scales and sample media [16-26].

In contrast, geochemical zonality (V_z) indicators such as Pb*Zn/Cu*Ag, Pb*Zn/Cu*Mo, and Pb*Zn*Bi/Cu*Mo*Ag were used to identify geochemical halos associated with blind porphyry copper deposits [27-30].

Nevertheless, focusing exclusively on metal concentration when investigating porphyry copper deposits may lead to erroneous results, particularly for weathered samples. For example, copper mineralization is possible in propylitic alterations. Mineralized veins and veinlets (such as sub-epithermal Zn-Cu-Pb-Ag-Au veins, and polymetallic veins) may also form at the porphyry copper deposit's margin.

Exotic copper mineralization may also occur due to the lateral migration of supergene solutions from porphyry copper deposits. Minor insignificant mineralization may create artificial anomalies in soil and stream sediment samples as a result of weathering. The algorithms could not identify these anomalies compared to anomalies found in the footprints of blind porphyry copper deposits.

(ii) Significant variation in the geochemical characteristics of rocks across a geological domain.

Several methods are existed for examining the geochemical changes while considering protolith composition include the following:

- Determining the abundance of elements of interest in comparison to the crustal average [31-32].
- Rationing single elements to immobile elements such as Ti, Y, or Zr [33-36].
- Calculating 'enrichment factors' using a relationship between two ratios, one representing a sample and the other representing average crustal abundance, in which the element concentration of interest is divided by the concentration of an immobile element [32, 37-45].
- Computing the mass balance establishes a baseline for determining element addition or loss based on the ratio of immobile to mobile elements in an altered and unaltered (or least-altered) sample [46-48].

The first two methods express relative values and do not quantify chemical changes, while the third method does not account for lithological variation. The fourth method, mass balance, considers the geology of the host rock and provides a quantified measure of chemical change.

The intensity and distribution of fluid-rock interactions can be mapped by observing the changes in mass caused by hydrothermal alteration in rocks [49]. By analyzing geochemical data, it is possible to determine the extent and spatial pattern of fluid-rock interactions, as alterations in mineralogy usually correspond to the amount of mass transferred during these interactions [50-54].

However, it is preferable to use unaltered or minimally altered samples for mass balance calculations as identifying samples of unaltered protolith rocks can be challenging, particularly at the prospect and deposit scales [55]. When there are numerous rock types, this process becomes more complicated. Additionally, certain porphyry copper districts are covered by soil due to the magmatic and meteoric water circulation, limiting the application of these methods.

This paper initially examines traditional soil geochemical signatures for exploring copper porphyry deposits. It discusses how they can lead to erroneous anomalies before extracting parameters to map anomalies related to blind copper porphyry mineralization based on the porphyry copper deposit (PCD) mineral system and fluid-rock interactions. A combination of pathfinder, immobile, and mobile elements is employed to find exploratory criteria to accomplish this goal. A statistical method based on fractal analysis was implemented to constrain the spatial extent of the soil geochemical haloes associated with the deposit.

2. Geological setting of the study area

The Kahang deposit was the first PCD discovered in the Urumieh-Dokhtar magmatic arc (UDMA) (Fig.1 a). This deposit is located in the center of Iran, northeast of the city of Isfahan. Tabatabaei and Asadi Haroni [56] divided the Kahang stock into three parts based on early lithogeochemical exploration (i.e., West, Central, and East). Later, the National Iranian Copper Industries (NICICO) expanded exploration in all three parts of the country, with more drilling conducted in the eastern region (Fig.1 b).

The Kahang deposit comprises quartz diorite, granodiorite, and dacite intruded into Eocene volcanic and volcaniclastic rocks, respectively [57-59]. In later stages, post-mineralization dikes crosscut the porphyry stocks. The measured deposits and indicated resources total 100 million metric tons (Mt) of sulfide ore with an average grade of 0.6% Cu and 70 ppm Mo. The new exploration program indicates the potential for an increase in the deposit resources base in the future.

Fig 2 depicts the swath plot of Cu, Mo, Pb, and Zn values from boreholes located within the pink square of Fig 1.b, indicating the presence of a large zone of copper-bearing anhydrite-quartz veinlet breccia 300–450m below the existing surface. By expanding drilling in the Kahang prospect, conventional methods direct exploration programs towards some minor anomalies.

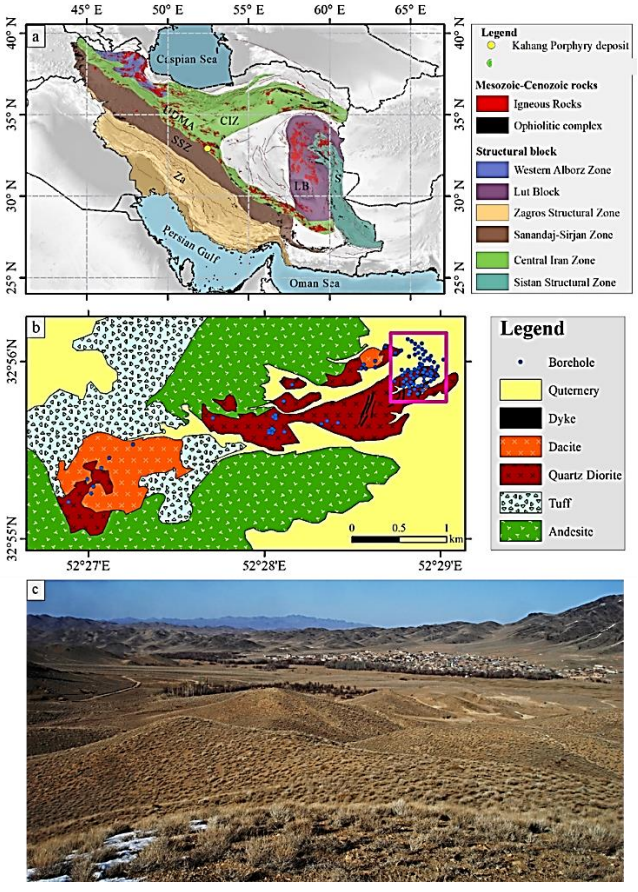

Figure 1. a) Location of Kahang porphyry copper deposit on the structural map of Iran. The location of the Kahang deposit is shown with a yellow circle. b) Simplified geological map of Kahang deposit, c) view of Kahang deposit area which covered by soil.

3. Geochemical data

A total of 2564 in situ soil samples were collected over a 3.1 km^2 area. The samples were taken at equal intervals of 25m in the NW-SE

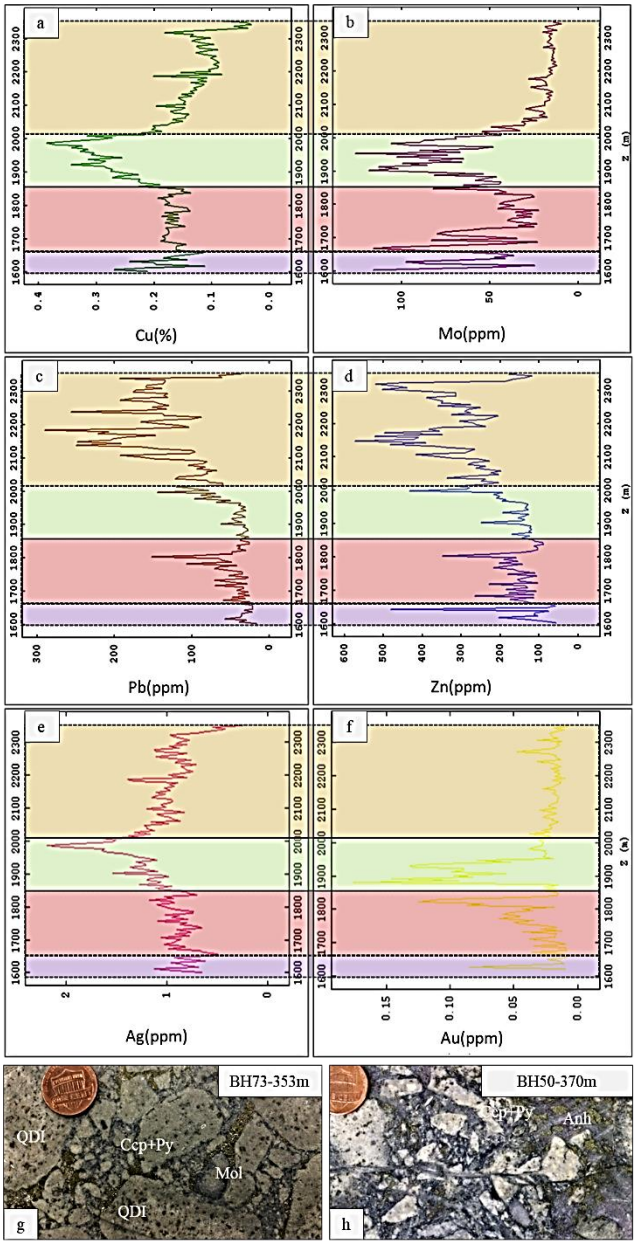

Figure 2. Swath plot of boreholes located in the pink square of Figure 1.b for a) Cu, b) Mo, c) Pb, d) Zn, e)Ag and f)Au. g) Rounded quartz diorite clasts cemented by chalcopyrite, molybdenite, and pyrite matrix. h) Anhydrite breccia with highly sericitized Quartz diorite clasts, cemented by anhydrite, chalcopyrite, and molybdenite matrix. Abbreviations: QDI= quartz diorite, Ccp= chalcopyrite, Py= pyrite, Mol= molybdenite, Anh= Anhydrite.

direction and 50m in the NE-SW direction along evenly spaced lines (Fig. 3). Each sample weighs about 300g, and their size distribution ranges between 250 and 400 micrometers. The locations of the samples are depicted in Figure 3.

The concentrations of 43 trace elements were determined using ICP-MS (for Ag, Al, As, Au, Ba, Be, Bi, Ca, Cd, Ce, Co, Cr, Cs, Cu, Fe, K, La, Li, Mg, Mn, Mo, Na, Nb, Ni, P, Pb, Rb, S, Sb, Sc, Sn, Sr, Te, Th, Ti, Tl, U, V, W, Y, Yb, Zn, and Zr) and a fire assay (for Au). Several studies have used these data to develop methods for detecting anomalies or as a geochemistry layer in potential mineral mapping [60-62].

As previously stated, Ag, Au, Cu, Mo, Pb, and Zn are used as pathfinder elements to investigate PCDs. Fig. 4 and table.3 depict the histograms and statistical summary for Ag, Au, Cu, Mo, Pb, and Zn. The figure demonstrates that the concentration distributions of all elements are positively skewed and exhibit a range of magnitudes.

Table 1 displays the detection limits for the elements. Additionally, a total of 28 samples were chosen and subjected to Thompson-Howarth error analysis [63-64] for quality assurance and quality control of the assay. The analytical error for Au, Ag, Al, Ca, Cu, Mo, Pb, and Zn can be found in Table 2. The outcomes indicate that the analytical method has yielded satisfactory error levels.

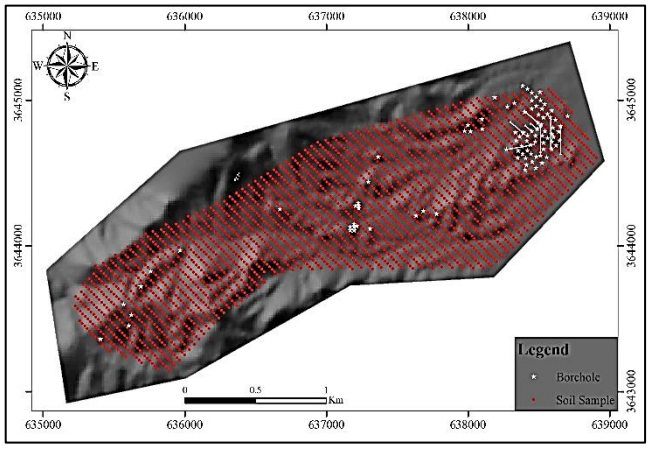

Figure 3. In situ soil samples and boreholes locations map of Kahang deposit.

4. Mineral reactions as proxies for addition and depletion patterns

To consider the mineral system, mineral reactions that may serve as proxies for the addition and depletion of elements in the host rock should be examined. The secondary process should then be evaluated in light of the sampling environment. Finally, the mappable spatial proxies for mineral potential mapping could be extracted by integrating these processes.

The effect of anhydrite formation on mass change could be explained by the large volume of anhydrite and sulfide veinlets found in the Kahang porphyry copper deposit [59]. The formation of anhydrite in PCDs is explained by the following gas-solid reactions [65]:

$$CaAl_2Si_3O_8 + 2SO_{2(g)} + 2H_{2(g)} \rightarrow CaSO_4 + Al_2SiO_{5(g)} + SiO_{2(g)} + H_2O_{(g)} + H_2S_{(g)} \quad (1)$$

The form's sulfide deposition reactions are driven by the rapid conversion of $SO_{2\ (g)}$ to $H_2S_{\ (g)}$.

$$CuCl_{2\ (g)} + FeCl_{2\ (g)} + 2H_2S_{\ (g)} \rightarrow CuFeS_2 + 4HCl_{\ (g)} \quad (2)$$

These reactions transform the host rock's Ca and Al into metastable minerals, such as anhydrite and andalusite [65]. The reactions are consistent with our petrographic observations and Afshooni's EMPA analysis of plagioclase [66], which indicates that the anhydrite immediately adjacent to the plagioclase undergoes sericite alteration along with Ca and Al reduction. The reaction (1) could occur in the upper portion of the mineralization core due to the volcanic eruption's flux of SO_2 as a reactive gas [67].

Anhydrite is highly soluble in cold water [68], whereas andalusite degrades during retrograde cooling [67]. Consequently, Ca and Al may deplete in soil samples from the upper part of the mineralization core. In contrast, Ca and Al in propylitic alteration are transformed into stable minerals such as chlorite, epidote, and calcite, which are all common constituents of the propylitic alteration assemblage.

Finally, based on fluid-rock interactions (i.e., syn-mineralization subsystem) and secondary process (i.e., post-mineralization subsystem), the Cu/(Al + Ca) index can be considered as mappable spatial proxies for delineating hydrothermal fluid interaction. Mineralization, alteration, and weathering in soil samples could all be considered using this ratio.

Table 1. Detection limits for analyzed elements.

Element	Ag	Al	As	Au	Ba	Be	Bi	Ca	Cd	Ce	Co
Unit	ppm	ppm	ppm	ppb	ppm	ppm	ppm	ppm	ppm	ppm	ppm
Detection limit	0.1	100.0	0.5	1.0	2.0	0.2	0.2	100.0	0.1	1.0	1.0
Element	Cr	Cs	Cu	Fe	K	La	Li	Mg	Mn	Mo	Na
Unit	ppm	ppm	ppm	ppm	ppm	ppm	ppm	ppm	ppm	ppm	ppm
Detection limit	1.0	0.5	1.0	100.0	100.0	1.0	1.0	100.0	5.0	0.5	100.0
Element	Nb	Ni	P	Pb	Rb	S	Sb	Sc	Sn	Sr	Te
Unit	ppm	ppm	ppm	ppm	ppm	ppm	ppm	ppm	ppm	ppm	ppm
Detection limit	1.0	1.0	10.0	1.0	1.0	50.0	0.5	0.5	0.5	2.0	0.1
Element	Th	Ti	Tl	U	V	W	Y	Yb	Zn	Zr	
Unit	ppm	ppm	ppm	ppm	ppm	ppm	ppm	ppm	ppm	ppm	
Detection limit	0.5	10.0	0.2	0.5	2.0	0.5	0.5	0.2	1.0	5.0	

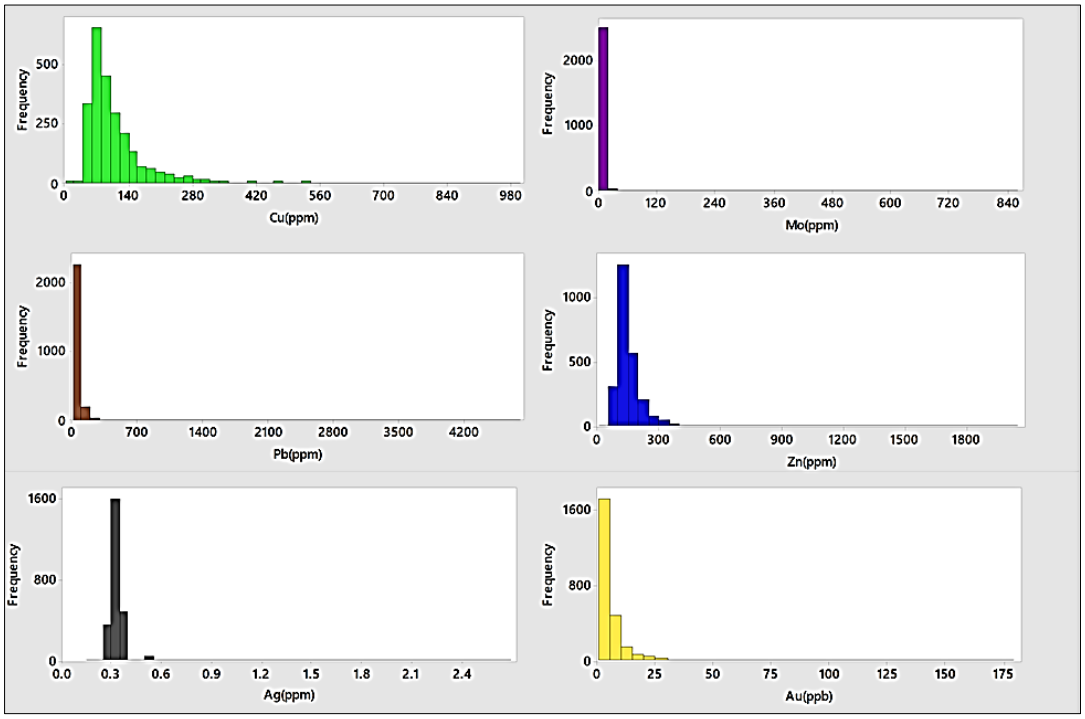

Figure 4. Histograms of raw Ag, Au, Cu, Mo, Pb, and Zn in soil samples of Kahang deposit.

Table 2. Analytical error for pathfinder elements (Au, Ag, Cu, Mo, Pb and Zn), Al and Ca.

Element	Average of original samples	Average of duplicate samples	Average difference	standard deviation	Analytical error
Ag	0.350	0.328	0.022	0.083	15.2%
Al	76301.857	90906.107	-14604.250	11465	5.9%
Au	24.906	36.750	-2.677	20.8	21.7%
Ca	34521.893	35835.857	-1313.964	9253	8.3%
Cu	328.607	373.107	-44.500	140.7	4.7%
Mo	3.528	5.217	-1.689	4.46	11.6%
Pb	43.286	38.893	4.393	18.9	14.9%
Zn	161.321	183.214	-21.893	48.8	7.4%

Table 3. Statistical summary of Cu, Mo, Pb, Zn, Ag and Au.

Element	min	1st quartile	median	mean	3rd quartile	max	range	Standard deviation
Cu (ppm)	2.3	68	90	124	134	988	985.7	106.3
Mo (ppm)	0.6	0.8	0.9	4.7	1	856	855.4	46.4
Pb (ppm)	10	37	47	69	68	4721	4711	128
Zn (ppm)	2	113	136	159	174	2042	2040	101
Ag (ppb)	0.18	0.3	0.32	0.33	0.34	2.67	2.49	0.1
Au (ppb)	0.75	2	4	7	8	179	178.25	10.5

5. Results

The Cu/(Al+Ca) index and standard method results in exploring porphyry copper deposits are presented in this section. The concentration-number fractal model was adopted, because it has a wide application and it is simple to implement in earth sciences [69-73]. Cu concentrations were divided into three populations using a C-N fractal model, with grades ranging from below 170 ppm to between 170 and 420ppm and more than 420ppm, respectively. Mo has three populations, according to the C-N fractal model.

The first population of Mo was discovered at grades below 10ppm, followed by the second population at grades between 10 and 25ppm, and the third population at concentrations greater than 25ppm. The Cu and Mo's C-N fractal model results appear to be the same as Afzal et al.'s spectrum–area fractal model [61].

Simple dot symbol maps were used to depict the distribution of Cu and Mo (Fig. 5). As can be seen, the district's central and northeast areas have the highest concentrations of Cu anomalies. A few of these anomalies were also discovered in the western and eastern regions of the study area. Anomalies have been discovered in the district's northeast and southwest quadrants.

On the other hand, (Pb*Zn)/(Cu*Mo) as the best general indicator of blind porphyry–Cu deposits [28, 74] was applied to examine levels of mineralization and their principal (supra-ore, upper-ore, ore, lower-ore, and sub-ore) halos [27, 75-76]. The range of 0.1 to 1 and 1 to 10 corresponds to the ore body level [29].

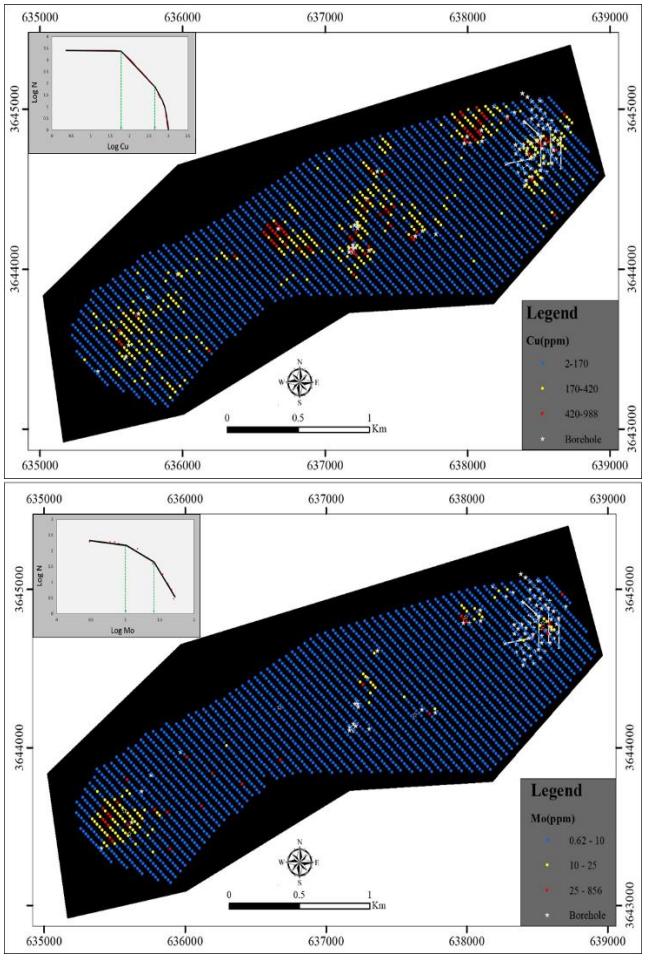

Figure 5. Cu and Mo distribution maps based on the C-N method in the Kahang deposit.

With this assumption, the study area can be subdivided into at least four zones, each of which contains possible porphyry–Cu deposits at varying depths (Fig. 6.a). Nonetheless, this zone may be an artifact for the reasons stated previously. Additionally, they continue to delineate extensive areas in the region of interest for exploratory borehole drilling.

As previously stated, when examining anomalies, fluid-rock interactions should be considered. The Cu/(Al+Ca) index was calculated based on an interpretation of the probable behavior of ore minerals. C-N fractal models reveal three distinct populations: those with values less than 0.001461, those with values between 0.001461 and 0.008, and those with values greater than 0.008. The third population with a Cu/(Al+Ca) ratio greater than 0.008 addressed two of the five potential zones (i.e., potentail zones 1 and 3) identified by the Cu and (Pb*Zn)/(Cu*Mo) maps (Fig 6.b).

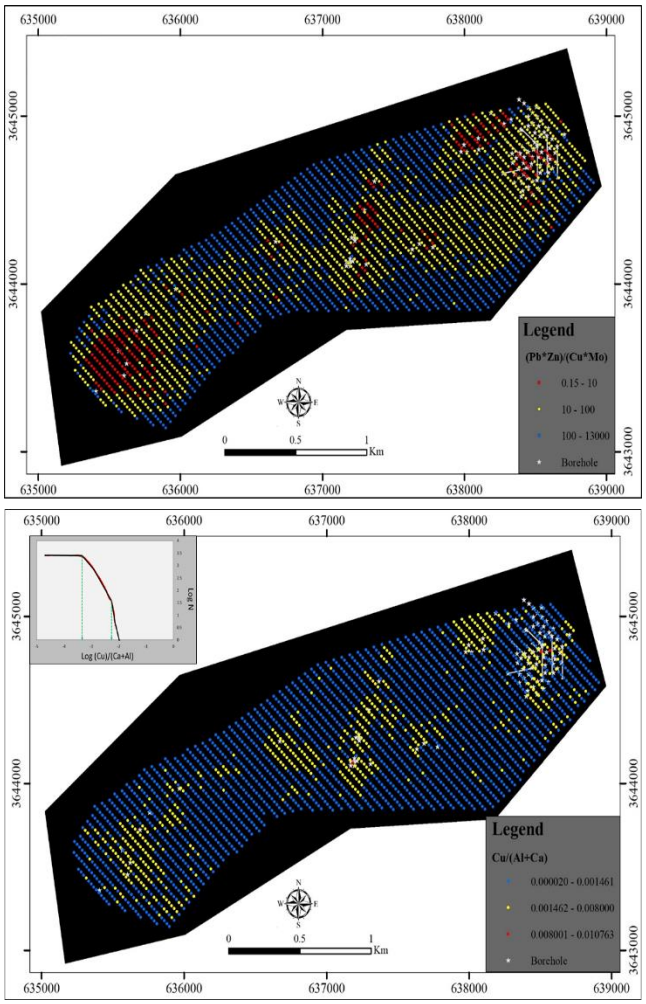

Figure 6. (Pb*Zn)/(Cu*Mo) and Cu/(Al+Ca) distribution maps in the Kahang deposit.

6. Discussion

In the Kahang district, soil anomalies were used to determine the magnitude and spatial distribution of probable outcropping or blind porphyry copper mineralization. Fig. 5 illustrates the distribution of Cu and Mo using a series of geochemical maps. Additionally, the geochemical zonality method concept enables the differentiation of upper to lower-ore anomalies (Fig 6.a). In Fig 7, the high-potential zone using the Cu, Mo, (Pb*Zn)/(Cu*Mo), and Cu/(Al+Ca) indexes was highlighted to facilitate a more effective comparison of anomalies.

This section compares the selection of high-potential zones for exploratory drilling using traditional geochemical data and fluid-rock interactions. The selection of pioneer exploratory boreholes in the initial attempt at ore exploration may affect the program's continuation.

This section also evaluates high-potential zones extracted using various methods from exploratory boreholes located on them. The term "productivity" was applied to provide a more precise definition of good and poor boreholes.

The following formula is used to define the productivity of each borehole [77]:

Productivity = Mean (%) * Thickness (m).

The threshold value (cut-off = 0.2%) corresponds to the economic cut-off value for Cu grade in ore reservoir modelling. Thus, increased productivity indicates a high-quality standard for exploratory boreholes (Table.4 and Fig. 8). Several boreholes (e.g., KAG01, KAG22, KAG25, KAG30, KAG68, and KAG77) are indicated by extremely low productivity and are located on superficial anomalies. In comparison, others have a high level of average productivity (e.g., KAG15 and KAG16).

Table 4. Borehole productivity.

BH name	mean (cut off= 0.2%)	Thickness (cut off= 0.2%)	mean * thickness (cut off= 0.2%)
KAG01	0.23	1	0.23
KAG15	0.57	242	137.94
KAG16	1.2	25	30
KAG22	0.24	1	0.24
KAG25	0	0	0
KAG30	0.26	99	25.74
KAG68	0.35	13	4.55
KAG77	0.28	48	13.44

The mineral system enables the evaluation of elemental changes associated with hydrothermal alteration via copper mineralization and the effect of secondary processes. This data was used to determine which parameters are most likely to provide the most reliable vectors toward copper mineralization.

The data were utilized to create meaningful haloes around ore formation and to propose pioneer boreholes. However, because Cu is used as the numerator, the Cu/(Al+Ca) index map is still affected by copper concentration, but true anomalies are highlighted compared to erroneous anomalies. Additionally, a few areas highlight the importance of drilling pioneer boreholes, which can assist exploration programs in locating blind mineralization more quickly.

7. Conclusion

In this paper, a ratio that is highly beneficial compared to simple pathfinder elements or known ratio maps is presented, based on the mineral system of the Kahang PCD and the possible behavior of elements in soil samples and weathered environments. This study applied a hybrid of pathfinder, immobile, and mobile elements in soil samples to determine an exploration ratio using the mineral system-based approach. In contrast, popular pathfinders could direct exploration programs towards high-potential areas within a porphyry copper prospect.

The productivity of exploratory boreholes was compared to validate the performance of the Cu/(Al+Ca) index. Furthermore, the study indicates that the Cu/(Al+Ca) index aids in detecting and further refining soil geochemical anomalies. Moreover, the Cu/(Al+Ca) index results are consistent with the porphyry mineral system and the effect of secondary processes in a weathered environment. The results suggest that the Cu/(Al+Ca) index can be used to identify credible geochemical anomalies in other similar mineralization systems.

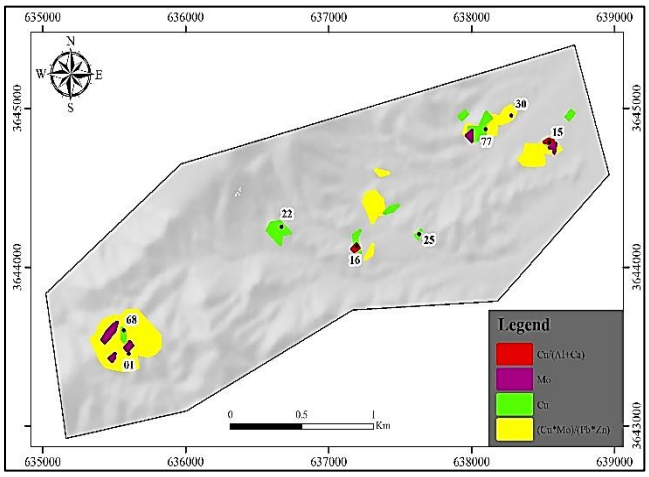

Figure 1: Cu, Mo, (Pb*Zn)/(Cu*Mo) and Cu/(Al+Ca) geochemical anomalies map and location of boreholes located on anomalies.

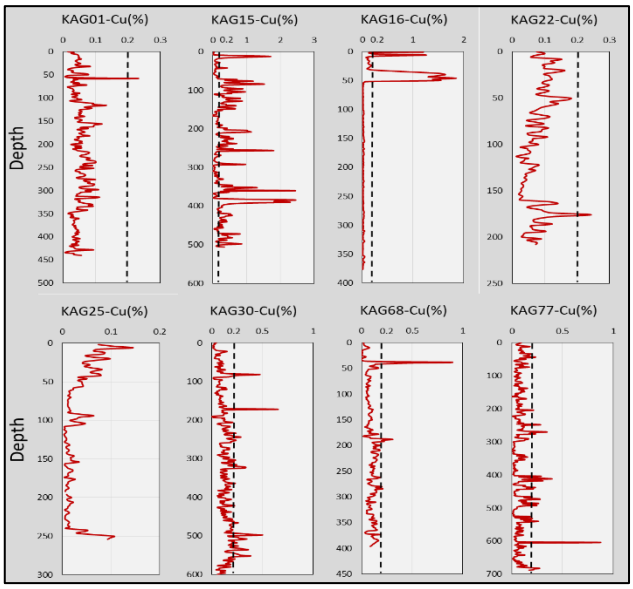

Figure 8. Copper grade variation in boreholes drilled in potential zones.

Acknowledgment

The authors gratefully acknowledge the management of National Iranian Copper Industries CO. (NICICo) and the management of the Kahang mine for their logistic support.

Conflict of interest statement

On behalf of all authors, the corresponding author states that there is no conflict of interest.

REFERENCES

[1] Wyborn LAI, Heinrich CA, Jaques AL (1994) Australian Proterozoic Mineral Systems: Essential Ingredients and Mappable Criteria. The AusIMM Annual Conference: 109–115.

[2] Knox-Robinson CM, Wyborn LAI (1997) Towards a holistic exploration strategy: using geographic information systems as a tool to enhance exploration. Aust J Earth Sci 44:453–463.

[3] Hagemann SG, Lisitsin VA, Huston DL (2016) Mineral system analysis: Quo vadis. Ore Geol Rev 76:504–522.

[4] Hronsky JMA (2004) The science of exploration targeting. SEG:129-133.

[5] Hronsky JMA, Groves DI (2008) Science of targeting: definition, strategies, targeting and performance measurement. Aust J Earth Sci 55:3–12.

[6] Kreuzer OP, Etheridge MA, Guj P, McMahon ME, Holden DJ (2008) Linking mineral deposit models to quantitative risk analysis and decision-making in exploration. Econ Geol 103:829–850.

[7] McCuaig TC, Beresford S, Hronsky J (2010) Translating the mineral systems approach into an effective exploration targeting system. Ore Geol Rev 38:128–138

[8] Yousefi M, Kreuzer OP, Nykänen V, Hronsky JM (2019) Exploration information systems–A proposal for the future use of GIS in mineral exploration targeting. Ore Geol Rev 111:103005.

[9] Skirrow RG, Murr J, Schofield A, Huston DL, van der Wielen S, Czarnota K, Coghlan R, Highet LM, Connolly D, Doublier M, Duan J (2019) Mapping iron oxide Cu-Au (IOCG) mineral potential in Australia using a knowledge-driven mineral systems-based approach. Ore Geol Rev 113:103011.

[10] Agnew PD, Muhling J, Goldfarb RJ (2004) Applications of geochemistry in targeting with emphasis on large stream and lake sediment data compilations. Predictive Mineral Discovery Under Cover: 232.

[11] Cohen DR, Kelley DL, Anand R, Coker WB (2010) Major advances in exploration geochemistry, 1998–2007. Geochem Explor Environ Anal 10(1):3–16.

[12] Reimann C (2005) Geochemical mapping: technique or art? Geochem-Explor Env A 5:359–370

[13] McKinley JM, Hron K, Grunsky EC, Reimann C, de Caritat P, Filzmoser P, van den Boogaart KG, Tolosana-Delgado R (2016) The single component geochemical map: fact or fiction? J Geochem Explor 162:16–28.

[14] Grunsky EC, de Caritat P (2020) State-of-the-art analysis of geochemical data for mineral exploration. Geochem Explor Env A 20(2):217-232.

[15] Brauhart CW (2019) The role of geochemistry in understanding mineral systems. ASEG Extended Abstracts 2019 (1): 1–5.

[16] Chen Y, An A, (2016) Application of ant colony algorithm to geochemical anomaly detection. J Geochem Explor 164:75–85.

[17] Zhao J, Chen S, Zuo R (2016) Identifying geochemical anomalies associated with Au–Cu mineralization using multifractal and artificial neural network models in the Ningqiang district, Shaanxi, China. J Geochem Explor 164: 54-64.

[18] Chen Y, Wu W (2019) Separation of geochemical anomalies from the sample data of unknown distribution population using Gaussian mixture model. Comput and Geosci 125:9-18.

[19] Zhang S, Xiao K, Carranza EJM, Yang F, Zhao Z (2019) Integration of auto-encoder network with density-based spatial clustering for geochemical anomaly detection for mineral exploration. Comput and Geosci 130:43-56.

[20] Ghezelbash R, Maghsoudi A, Carranza EJM (2020) Optimization of geochemical anomaly detection using a novel genetic K-means clustering (GKMC) algorithm. Comput and Geosci 134:104335.

[21] Li H, Li X, Yuan F, Jowitt SM, Zhang M, Zhou J, Zhou T, Li X, Ge C, Wu B (2020) Convolutional neural network and transfer learning based mineral prospectivity modeling for geochemical exploration of Au mineralization within the Guandian–Zhangbaling area, Anhui Province, China. Appl. Geochemistry 122:104747.

[22] Li B, Liu B, Wang G, Chen L, Guo K (2021) Using geostatistics and maximum entropy model to identify geochemical anomalies: A case study in Mila Mountain region, southern Tibet. Appl. Geochemistry 124:104843.

[23] Luo Z, Xiong Y, Zuo R (2020) Recognition of geochemical anomalies using a deep variational autoencoder network. Appl Geochemistry 122:104710.

[24] Wang J, Zhou Y, Xiao F (2020) Identification of multi-element geochemical anomalies using unsupervised machine learning algorithms: A case study from Ag–Pb–Zn deposits in north-western Zhejiang, China. Appl Geochemistry 120:104679.

[25] Xiong Y, Zuo R (2020) Recognizing multivariate geochemical anomalies for mineral exploration by combining deep learning and one-class support vector machine. Comput and Geosci 140:104484.

[26] Wheeler S, Henry T, Murray J, McDermott F, Morrison L (2021) Utilising CoDA methods for the spatio-temporal geochemical characterisation of groundwater; a case study from Lisheen Mine, south central Ireland. Appl Geochemistry 127:104912.

[27] Grigorian SV (1992) Mining Geochemistry. Nedra Publishing House, Moscow.

[28] Ziaii M, Abedi A, Ziaei M (2009) Geochemical and mineralogical pattern recognition and modeling with a Bayesian approach to hydrothermal gold deposits. Appl Geochemistry 24:1142–1146.

[29] Ziaii M, Carranza EJM, Ziaei M (2011) Application of geochemical zonality coefficients in mineral prospectivity mapping. Comput and Geosci 37(12):1935-1945.

[30] Talesh Hosseini S, Asghari O, Ghavami Riabi SR (2018) Spatial modelling of zonality elements based on compositional nature of geochemical data using geostatistical approach: a case study of Baghqloom area, Iran. Journal of Mining and Environment 9(1):153-167.

[31] Govett GJS (1983) Handbook of Exploration Geochemistry. Elsevier.

[32] Brauhart CW, Grunsky EC, Hagemann SG (2017) Magmato-hydrothermal space: a new metric for geochemical characterisation of metallic ore deposits. Ore Geol Rev 86:867–895.

[33] Winchester JA, Floyd PA (1977) Geochemical discrimination of different magma series and their differentiation products using immobile elements. Chem Geol 20:325–343.

[34] MacLean W, Barrett T (1993) Lithogeochemical techniques using immobile elements. J Geochem Explor 48:109–133.

[35] Rollinson HR (1993) Using Geochemical Data: Evaluation, Presentation, Interpretation. Routledge, Longman, Harlow.

[36] Brand NW (1999) Element ratios in nickel sulphide exploration: vectoring towards ore environments. Geochem Expl 67:145–165.

[37] Chandrajith R, Dissanayake C, Tobschall H (2001) Application of multi-element relationships in stream sediments to mineral exploration: a case study of Walawe Ganga Basin, Sri Lanka. Appl Geochem 16:339–350.

[38] El-Makky AM, Sediek KN (2012) Stream sediments geochemical exploration in the northwestern part of Wadi Allaqi Area, South Eastern Desert, Egypt. Nat Resour Res 21:95–115.

[39] Gong Q, Deng J, Wang C, Wang Z, Zhou L (2013) Element behaviors due to rock weathering and its implication to geochemical anomaly recognition: a case study on Linglong biotite granite in Jiaodong peninsula, China. J Geochem Explor 128:14–24.

[40] Yaylalı-Abanuz G (2013) Determination of anomalies associated with Sb mineralization in soil geochemistry: a case study in Turhal (northern Turkey). J Geochem Explor 132:63–74.

[41] Wang C, Carranza EJM, Zhang S, Zhang J, Liu X, Zhang D, Sun X, Duan C (2013) Characterization of primary geochemical haloes for gold exploration at the Huanxiangwa gold deposit, China. J Geochem Explor 124:40–58.

[42] Liu C, Hu S, Ma S, Tang L (2014) Primary geochemical patterns of Donggua Mountain laminar skarn copper deposit in Anhui, China. J Geochem Explor 139:152–159.

[43] Hosseini-Dinani H, Aftabi A, Esmaeili A, Rabbani M (2015) Composite soil-geo-chemical halos delineating carbonate-hosted zinc-lead-barium mineralization in the Irankuh district, Isfahan, west-central Iran. J Geochem Explor 156:114–130.

[44] Chen Z, Chen J, Tian S, Xu B (2017) Application of fractal content-gradient method for delineating geochemical anomalies associated with copper occurrences in the Yangla ore field, China. Geosci Front 8:189–197.

[45] Carranza EJM (2017) Geochemical Mineral Exploration: should we use enrichment factors or log-ratios? Nat Resour Res 26:411–428.

[46] Gresens RL (1967) Composition-volume relationships of metasomatism. Chem Geol 2:47–65.

[47] Grant JA (1986) The isocon diagram; a simple solution to Gresens' equation for meta-somatic alteration. Econ. Geol. 81, 1976–1982.

[48] Grant JA (2005) Isocon analysis: a brief review of the method and applications. Phys. Chem Earth 30:997–1004.

[49] Gaillard N, Williams-Jones AE, Clark JR, Salvi S, Perrouty S, Linnen RL, Olivo GR (2020) The use of lithogeochemistry in delineating hydrothermal fluid pathways and vectoring towards gold mineralization in the Malartic district, Québec. Ore Geol Rev 120:103351.

[50] Bierlein FP, Fuller T, Stüwe K, Arne DC, Keays RR (1998) Wallrock alteration associated with turbidite-hosted gold deposits: examples from the Palaeozoic Lachlan Fold Belt in central Victoria, Australia. Ore Geol Rev 13:345–380.

[51] Eilu P, Mikucki JE, Dugdale LA (2001) Alteration zoning and primary geochemical dispersion at the Bronzewing lode-gold deposit, Western Australia. Miner Deposita 36:13–31.

[52] Whitbread MA, Moore CL (2004) Two lithogeochemical approaches to the identification of alteration patterns at the Elura Zn–Pb–Ag deposit, Cobar, New South Wales, Australia: use of Pearce Element Ratio analysis and Isocon analysis. Geochem-Explor Env A 4:129–141.

[53] Warren I, Simmons SF, Mauk JL (2007) Whole-Rock Geochemical Techniques for Evaluating Hydrothermal Alteration, Mass Changes, and Compositional Gradients Associated with Epithermal Au-Ag Mineralization. Econ Geol 102:923–948.

[54] Prendergast K (2007) Application of lithogeochemistry to gold exploration in the St Ives goldfield, Western Australia. Geochem-Explor Env A 7:99–108.

[55] Ahmed AD, Hood SB, Gazley MF, Cooke DR, Orovan EA (2019) Interpreting element addition and depletion at the Ann Mason porphyry-Cu deposit, Nevada, using mapped mass balance patterns. J Geochem Explor 196:81-94.

[56] Tabatabaei SH, Asadi Haroni H (2006) Geochemical characteristics of Gor Gor Cu–Mo porphyry system. Iranian Symposium on Geosciences: 60.

[57] Afshooni SZ, Mirnejad H, Esmaeily D, Haroni HA (2013) Mineral chemistry of hydrothermal biotite from the Kahang porphyry copper deposit (NE Isfahan), Central Province of Iran. Ore Geol Rev 54:214-232.

[58] Azadi M, Mirmohammadi M, Hezarkhani A (2015) Aspects of magmatic–hydrothermal evolution of Kahang porphyry copper deposit, Central Iran. Arab J Geosci 8(7):4873-4893.

[59] Hajsadeghi S, Mirmohammadi M, Asghari O (2021) Evidence of gas plume model in porphyry copper deposits based on anatomy, fluid inclusions and HO isotopes: Insight from Kahang deposit, Iran. Ore Geol Rev 104517.

[60] Harati H (2011) Geology, alteration, mineralogy, and geochemical investigation of the intrusive bodies in the Kahang porphyry copper deposit, northeast of Isfahan. Dessertation. Islamic Azad University, Tehran Branch.

[61] Afzal P, Harati H, Alghalandis YF, Yasrebi AB (2013) Application of spectrum–area fractal model to identify of geochemical anomalies based on soil data in Kahang porphyry-type Cu deposit, Iran. Chem Erde 73(4):533-543.

[62] Barak S, Imamalipour A, Abedi M, Bahroudi A, Khalifani FM (2021) Comprehensive modeling of mineral potential mapping by integration of multiset geosciences data. Chem Erde: 125824.

[63] Thompson M, Howarth RJ (1976) Duplicate analysis in practice – Part 1. Theoretical approach and estimation of analytical reproducibility. The Analyst 101:690–698.

[64] Thompson M, Howarth RJ (1978) A new approach to the estimation of analytical precision. J Geochem Explor 9:23–30.

[65] Henley RW, King PL, Wykes JL, Renggli CJ, Brink FJ, Clark DA, Troitzsch U (2015) Porphyry copper deposit formation by sub-volcanic sulphur dioxide flux and chemisorption. Nat Geosci 8(3):210-215.

[66] Afshooni SZ (2013) Study of alteration zones on the intrusive and volcanic rocks of the Kahang exploration area (NE Isfahan) with especial reference to Cu-Mo mineralization, Dissertation, University of Tehran.

[67] Henley RW, Seward TM (2018) Gas–solid reactions in arc volcanoes: Ancient and modern. Rev. Mineral Geochem 84(1):309-349.

[68] Dickson FW, Blount CW, Tunell G (1963) Use of hydrothermal solution equipment to determine the solubility of anhydrite in water from 100 degrees C to 275 degrees C and from 1 bar to 1000 bars pressure. Am J Sci 261(1):61-78.

[69] Mao, Z.L., Peng, S.L., Lai, J.Q., Shao, Y.J. and Yang, B., 2004. Fractal study of geochemical prospecting data in south area of Fenghuanshan copper deposit, Tongling Anhui. Journal of Earth Sciences and Environment. 26(4), 11-14.

[70] Hassanpour S, Afzal P (2013) Application of concentration–number (C–N) multifractal modeling for geochemical anomaly separation in Haftcheshmeh porphyry system, NW Iran. Arab J Geosci 6(3):957-970.

[71] Kurdi M, Soltani-Mohammadi S, Eslamkish T, Larina N (2017) Evaluating the performance of concentration-number (CN) fractal model for separation of soil horizon regarding vertical distribution and 3D models. JTethys 5(4):337-349.

[72] Hajsadeghi S, Asghari O, Mirmohammadi M, Afzal P, Meshkani SA (2020) Uncertainty-volume fractal model for delineating copper mineralization controllers using geostatistical simulation in Nohkouhi volcanogenic massive sulfide deposit, Central Iran. Bull Min Res Exp 161(161):1-11.

[73] Darvishi S, Farhadinejad T, Aliabadi M, Asgari A (2021) Separation of Au, Ag, As, Cd, Cu, Hg, Mo and Sb geochemical anomalies using the concentration-number (CN) fractal and classical statistical models in Nahavand 1: 100,000 sheet, Iran. Arab J Geosci 14(5):1-14.

[74] Ziaii M (1996) Lithogeochemical Exploration Methods for Porphyry Copper Deposit in Sungun, NW Iran. M.Sc. Thesis, Moscow State University.

[75] Solovov AP (1987) Geochemical Prospecting for Mineral Deposits. Mir, Moscow.

[76] Solovov AP (1990) Handbook on Geochemical Prospecting for Useful Minerals. Nedra Publishing House, Moscow.

[77] Hosseini SA, Abedi M (2015) Data envelopment analysis: a knowledge-driven method for mineral prospectivity mapping. Comput and Geosci 82:111-119.